CALCULATION OF THE DYNAMIC RESPONSE OF REACTOR CONTAINMENT SYSTEMS TO FULL CORE EXPLOSIONS

M.S. COWLER, N.E. HOSKIN, A.G. ROWLINSON

United Kingdom Atomic Energy Authority,
Atomic Weapons Research Establishment, Aldermaston, Reading, Berkshire, RG7 4PR,
United Kingdom

SUMMARY

ASTARTE, a comprehensive time-dependent two-dimensional Lagrangian hydrodynamic code has been developed within the UKAEA to determine numerically the loadings and strains arising within the primary containment system following a high energy reactor excursion. The detail, both temporal and spatial, which is achievable by judicious use of such a code allows the safety analyst to examine the response of individual sections of the containment. It is possible, furthermore, to predict the effects on the history of a given reactor accident of variations in the basic characteristics of the components making up the containment system.

To validate this approach an extensive analysis, using ASTARTE, has been made of model excursion experiments for a single tank pool-type reactor system, carried out at AWRE, Foulness, England; (see: N.J.M. Rees: A Model Investigation of Explosion Containment in Single Tank Fast Reactors: Proc. Conf. on Safety, Fuels and Core Design in Large Fast Power Reactors, Argonne, USA, October 1965).

These experiments, contained in an overstrong tank partly filled with water, included both bare explosive charges and charges confined within a simulated reactor structure. An extensive coverage of the system was achieved with pressure transducers located on the walls and over the roof so that the complete history of the experiment could be followed. Results of calculations on the bare charge experiments, have demonstrated clearly the ability to accurately reproduce numerically the measured loadings and impulses around the confining tank; (see: N.E. Hoskin, M.W.S. Mawbey and N.J.M. Rees: Calculation of the Dynamic Response of Reactor Containment Systems: Conf. on Engineering of Fast Reactors for Safe and Reliable Operation. Karlsruhe, Germany, October 1972).

The investigation has been extended to examine the tests involving confined charges and the present paper discusses the results obtained from this analysis. The effect of the confinement on the coolant flow is examined and, inter alia, an explanation is found for the rather surprising result that the impulse on the roof is increased when the explosive charge is confined within the reactor structure simulant. The relatively massive diagrid plate structure has a significant effect on the directional distribution of outward energy propagation and this is discussed. Considerable emphasis is placed on the necessity to define accurately the constitutive relations, determining the stress-strain behaviour, of all components included in the simulated reactor system.

The calculations on the model test geometry are extended by replacing the energy release from an explosive charge by a UO_2 vapour explosion resulting from a Bethe-Tait energy release. The differences and similarities between loadings produced by the two methods of energy release are discussed at some length. The histories of the two accident calculations will be illustrated graphically on a short film.

1. Introduction

The increasing power of available computers over recent years has improved the feasibility of using computer codes to determine numerically the loadings and strains arising within a primary reactor containment system during a high-energy excursion. It is not surprising, therefore, that the different fast reactor projects have each developed large-scale codes to analyse the different phases of an accident history. The period immediately following a nuclear energy release is one characterised by energy distribution by wave propagation, while subsequently the dominant mode of energy distribution changes to coolant momentum (see e.g. Fistedis [1]). An extensive knowledge of methods of solution of 2-D unsteady compressible fluid flow problems exists, mainly by Lagrangian finite difference schemes. These are ideal for the determination of the initial phase of the accident history and examples developed for reactor accident analysis are the Interatom code, ARES [2], the ANL code, REXCO-H [3], and the UKAEA code, ASTARTE [4]. These are all similar in structure and differ mainly in the boundary conditions and variety of constitutive relations considered. The development of codes suitable for considering the coolant momentum flow has not reached the same level of sophistication and current development is extensive by all projects (Egleme [6], Denise [7]). However, this phase will not be considered in the present paper, where attention will be concentrated on investigating phenomena in the initial phase using the UKAEA Lagrangian code, ASTARTE, and demonstrating the effects of variations in the basic characteristics assumed for the components of the containment system on the overall flow behaviour.

In order to validate this approach using ASTARTE, an analysis in depth has been made of model excursion experiments for a single pool-type reactor system performed at AWRE, Foulness, England [8]. The experiments, contained in an overstrong tank partly filled with water, included both bare explosive charges and charges confined within a simulated reactor structure. Loading histories were obtained from numerous pressure transducers located on the walls and roof. These experimental results have also been used in the validation of REXCO-H (see Ash [3]) and ARES (Doerbecker [2]) and clearly demonstrate the usefulness of well-instrumented experiments for such purposes. Comprehensive results of ASTARTE calculations based on the experiments containing a bare charge have been reported elsewhere (Hoskin et al [5]), where brief reference is made to an initial calculation based on the experiments involving a confined charge. Further calculations involving the confined charge were delayed at that time until constants for a more sophisticated constitutive equation for the compaction of distended materials were derived for both the confining materials. It was also necessary to complete the inclusion of a mesh stabilisation scheme in ASTARTE, in order to allow the calculations to proceed realistically as far as times of coolant impact on the roof. These developments have since been completed and further analysis performed on the experiments involving the confined charge. The present paper discusses these results, together with results of calculations on the model test geometry where the energy release from the explosive charge was replaced by a UO_2 vapour explosion resulting from a Bethe-Tait energy release. This is not intended to simulate a true reactor incident but is included to illustrate differences in loadings arising from the differing forms of energy release.

2. Description of the Experimental Geometry

A detailed description of the experiments under analysis has been previously given by Rees [8]. An extensive coverage of the system was achieved with pressure transducers located

on the walls and over the roof so that the complete history of the experiments could be followed (see figure 1). The confined charge was contained in an axisymmetric system designed to simulate a core/breeder structure (figure 2).

For the calculations performed by ASTARTE, the structure was represented by dividing the system into a Lagrangian grid of mesh points within which a simplified model of the confinement was generated as indicated in figure 3(a). The tensile strength of the thin steel containing vessel was neglected in the present calculations because of its complex shape and difficulties in determining its dynamic properties, but it is recognised that internal shells within a reactor structure may contribute a vital part in the energy-absorbing characteristics of the system. However, the influence of the relatively massive diagrid structure supporting the charge was investigated by assuming a rigid support to the charge in some of the calculations. In all calculations, the explosive charge was assumed to detonate at its mid point and standard procedures for burning explosive were used (see e.g. Wilkins [9]).

3. Constitutive Equations

The equation of state of water currently in use within the U.K. has been described previously for the calculations based on the experiments including a bare charge (Hoskin et al [5]). Since both the lead shot and the graphite surrounding the charge in the experiments involving a confined charge were initially distended, an equation of state for distended or porous materials was used to describe their compaction behaviour. The initial calculation on the geometry including the confined charge described in the earlier paper employed an elastic perfectly-plastic locking (EPPL) model (Linde and Schmidt [10]) while subsequent calculations reported in the present paper used a more sophisticated model first proposed by Herrmann [11]. The main characteristics of the two models are illustrated in figure 4. Both models assume compaction to the solid material, but whereas in the EPPL model the porous material compacts to solid density with no increase in stress once the Hugoniot elastic limit is reached (i.e. ignoring any strength of partially compacted material), the Herrmann model permits the distended material to support a variable and increasing elastic-plastic stress during compaction to the fully collapsed state.

Following the inclusion in ASTARTE of the Herrmann model for distended materials, the original calculation on the geometry including the confined charge was repeated with improved equations of state for the lead shot and graphite. The constants for both the EPPL and Herrmann models were chosen so that physical quantities such as initial density, elastic wave velocity and Hugoniot elastic limit were identical in both models. The effect of using the Herrmann model to describe these materials is shown in figure 5 for the early stages of the excursion, where the pressure histories at gauge 3 are given for both calculations together with the experimental record. Whereas in the initial calculation, using the EPPL model, the predicted peak pressure was 30% too low, much better agreement with the experimental record was obtained using the Herrmann model, the peak pressure now being slightly overestimated. The predicted arrival time and the pulse width agreed well with experiment in both calculations.

4. The Effect of the Diagrid

In the experiments, the confined charge was supported on a relatively massive diagrid structure which would have a significant effect on the directional distribution of outward

energy propagation. Since the deformation of such a structure cannot be described in detail by ASTARTE at present, its overall effect was estimated by performing a calculation in which the diagrid and its supports were treated as a completely rigid structure. This extreme simplification should not, in fact, be far from reality since the diagrid was very strong and suffered little distortion during the experiment. It did however break away from the remaining structure and was driven to the bottom of the tank. Other calculations (see section 6.2.1) showed that relaxation of the rigidity of the support below the diagrid had some effect. However it is not known when the break away occurred during the experiment so arbitrary refinements, such as allowing the diagrid to collapse at a preassigned time, were not examined. The results of the calculation with diagrid and supports both rigid are compared with those of the previous calculation in figure 6. In this figure the pressure histories and impulse-time curves are given at gauge 3 for the two calculations, together with the experimental record. Both calculations used the Herrmann model to describe the confining materials. The agreement is seen to be particularly good for the calculation with a rigid diagrid and supports. In the calculation with no diagrid the second pressure peak, produced by the reflected shock off the bottom of the tank, appears slightly higher than the experimental record while the dip between the two peaks fails to be reproduced. The total impulse for the calculation with a rigid diagrid and supports agreed exceptionally well with the experimental record in both cases.

5. Mesh Stabilisation

In order to realistically continue the calculations discussed so far to times of coolant impact and subsequent pressure loadings on the roof any gross mesh distortions, characteristic of Lagrangian codes, had to be eliminated without introducing large errors into the true solution. In ASTARTE, a mesh stabilisation scheme developed at Los Alamos (Butler [12]) has been used. The scheme is essentially a Hooke's Law force with damping that tends to keep a vertex at the centre of mass of its eight adjacent neighbours. The additional acceleration on a given vertex is of the form

$$\underline{A}_i = \kappa^2 \sum_j (\underline{r}_j - \underline{r}_i) + 2\kappa \sum_j (\underline{u}_j - \underline{u}_i)$$

where the summation over j includes the eight neighbouring vertices. The parameter κ depends upon the particular problem and must be chosen so that mesh distortions are acceptable but the overall dynamics are not altered. Tests were performed on the calculations involving both the bare and confined charge to obtain a suitable value for κ. These tests showed that a value κ = 20 (in MKS units) had no effect on the calculated pressure-time histories at gauge positions on the wall, but limited mesh distortions to a tolerable level. This value of κ was used in all subsequent calculations requiring mesh stabilisation (in the earlier report (Hoskin et al [5]), this value was erroneously quoted as κ = .02, in MKS units). In all such calculations, the stabilising forces only became operative after the initial shock had propagated away. If operative from time zero, the restraining accelerations become too large at meshes being traversed by the initial shock, resulting in excessive confinement of the charge.

6. Results of Calculations and Comparison with Experiment

The results discussed so far clearly indicated that the ASTARTE calculation which included a rigid diagrid and supports was giving the best agreement with the experiments. This calculation was therefore continued to obtain the times of coolant impact and the subsequent pressure loadings on the roof. Mesh stabilisation was included in the meshes containing the explosive products after the first 250 μsecs and the stabilised region was extended to include the lead shot after 1 msec.

Fairly complicated spall behaviour of the water, as described in the earlier report, was allowed. Thus, if tensions greater than the prescribed maximum of 25 bars occurred, spalling was permitted along predefined mesh lines in the upper layers of the water (see figure 3(b)). Neglect of this behaviour produces significant differences in the velocity of the free surface and hence the start of loading on the roof.

6.1 Graphical Output

Much of the output from the ASTARTE calculation was obtained in graphical form showing mesh distortions (figure 3) or pressure and velocity distributions. The overall flow can then be followed visually as illustrated in figure 8 where pressure and velocity distributions are shown for six epochs of the calculation. It is seen that the primary shock produced by detonation of the explosive radiates outward through the confinement and is reflected from the tank wall and bottom (figure 8(a)). As the two reflected shocks interact, a high pressure area is formed at the bottom of the tank (figure 8(b)).

The action of the confinement is now to prevent any reverse flow of energy and momentum inwards towards the central explosive region and to direct the flow upwards towards the roof. (This is in contrast to the fluid flow in the experiment with an unconfined charge where the bubble of explosive products was in a collapsing phase after the first few hundred μsecs.) As a result of this the entire coolant flow is directed vertically towards the roof at an early stage in the experiment (see figure 8(b)). After 1 msec almost the entire volume of water is at zero pressure or in slight tension, and most of the energy of the system is in fluid momentum in a vertical direction (figure 8(d)). The water is seen to spall immediately above the confinement at this stage and the degree of spalling increases as the coolant approaches the roof. A second spall appears just prior to the initial impact of the water on the roof (figure 8(e)), which occurs at 1450 μsecs. The spalling included is relatively crude and is determined by the size of mesh. It is probable that further spall planes should be included to reproduce the true free surface motion.

6.2 Numerical Output

The numerical output for the ASTARTE calculation was mainly in the form of pressure-time histories at the twelve gauge positions shown in figure 1. These histories were integrated to derive impulse-time curves in order to minimise the effect of extraneous oscillations in both numerical and experimental records. The results at gauge 3 for the present calculation have been previously discussed in section 4 (see figure 6), where a comparison was made with a calculation which neglected the effect of the diagrid. Good agreement was obtained between the experimental and calculated pressure histories and the impulse-time curves agreed exceptionally well. Figure 8 shows comparisons of both pressure and impulse at gauges 1, 6, 11 and 12 respectively. These will be discussed in detail to illustrate points which may be deduced from the analysis.

6.2.1 Gauge 1

Gauge 1 recorded details on the wall very near to the bottom of the tank (see figure 1). The calculation did not predict the experimental record at this gauge to the same accuracy as was achieved at gauge 3. The arrival time of the pulse, the initial peak pressure and the pulse duration were predicted very well but the calculation failed to reproduce the attenuation of the experimental pressure record following this peak. Consequently the predicted impulse on the wall at that point was 50% too high. A second calculation in which the rigidity of the supports to the diagrid was relaxed reduced the spiky pressure peak in the latter part of the pulse but the reduction was not sufficient to give satisfactory agreement.

Failure to reproduce the attenuation of the experimental record is believed due to incorrect modelling of the release behaviour of the confining graphite region (changes here would modify the late part of the pressure record at gauge 1) or the inability to reproduce the impulsive jumping of the whole confinement system off the bottom of the tank. The confinement merely rests on the bottom of the tank and because it is not a balanced system it is thought probable that it will levitate at some stage in the experiment. Unfortunately there were no gauges on the bottom to prove or disprove this hypothesis and no way, in a Lagrangian code, to accurately reproduce such a motion. In view of the good agreement at other gauges (see below) no further efforts have been made to resolve this disagreement.

6.2.2 Gauge 6

It will be seen that this gauge is in the wall and lies just below the water surface. It therefore records the arrival of the initial wave through the water and the high pressure resulting from impact of the water on the roof. The initial arrival of the wave is predicted well in time, magnitude and duration but the calculated free surface velocity is too low and the large pressure pulse caused by water impact on the roof is later than in the experiment. Nevertheless the final computed impulse is within 15% of the measured value and this agreement is thought satisfactory.

6.2.3 Gauge 11

This gauge lies in the roof at the centre of the core plug. The experimental record has two large pressure spikes with only insignificant pressures recorded between the spikes. This is highly suggestive of spalling at the water surface and as discussed in section 6.1 the calculation showed that spalling occurred over a considerable period of time as the water moved towards the roof. A calculation was made without permitting this spalling, in order to determine the effect and the calculated arrival time at the gauge was delayed by over 100 μsec. It is seen that the calculation, even with spalling included, still does not match the experiment exactly but it is thought that finer definition in both mesh size and number of spall planes near the surface would improve the agreement if it were thought necessary. Although the shape of the experimental pressure record is not reproduced (with the relatively crude mesh definition it is asking a lot to reproduce pressure spikes less than 50 μsec in duration) the computed impulse is within 25% of the measured value.

6.2.4 Gauge 12

This gauge lies on the edge of the core plug but it is difficult to explain the early pressure spike at 1.3 msec in the experimental record since this is not matched with a similar spike at gauge 11. The first spike at gauge 11 at 1.5 msec can probably be correlated

with the second spike at gauge 12 and the computed arrival time at gauge 12 agrees with this to within 100 μsec approximately. The computed impulse agrees very well with the experimental value so, since the agreement at gauge 11 was also quite good, the integrated impulse over the surface of the core plug would obviously be predicted accurately.

6.3 Overall Comparison

Considering figure 9, together with the comparison of gauge 3 in figure 6 we see that there is an encouraging agreement in overall behaviour at all gauge positions except for the later part of the pressure history at gauge 1. The predicted free surface velocity of the water is too low so that the computed time of impact of the water on the roof is late compared with experiment. The inclusion of spalling at the free surface improved the agreement on the core plug but not on the outer parts of the roof. Predicted impulses on the wall and roof, except at gauge 1 agreed well with experiment.

7. The Effect of Sliding in the Confinement

The upper region of the confinement was in the form of a sand-filled canister (represented in the calculations by graphite since the initial densities and compaction behaviour are not too dissimilar) which was only lightly attached to the steel containing vessel. Some doubt existed as to whether or not this part of the confinement might be projected vertically towards the roof early in the experiment. This would accelerate the water directly above the canister, increasing the resulting roof loadings. A calculation was performed in which this region was free to move independently of the rest of the confinement (this was achieved by allowing sliding in the vertical direction). The movement during the times considered was found to be small and made no difference to the final loadings on the roof.

The results of a similar calculation, in which horizontal sliding along the top of the diagrid was permitted, also showed that the loading histories on the wall and roof were not significantly altered.

It seems clear therefore, from these two calculations, that differential motion of separate parts of the confinement has no significant effect on the loadings and that only wave propagation effects through the confinement and momentum of the coolant need be considered.

8. Effect of Charge Confinement

Rees [8] concluded in his original investigation that the effect of surrounding the explosive charge by a model breeder structure was, in the case of a light-gauge outer tank, to direct the energy release upwards to the tank roof and core plug, resulting in higher plug-ejection velocity. Comparison of the present calculations with those for a bare charge reported in Hoskin et al [5] show that the same is true for the experiments with an overstrong outer tank. The effect of the confinement is to direct the coolant flow entirely towards the roof at a very early stage of the calculation (see figure 8(b)). Pressure and velocity distributions at two times during the earlier calculation involving a bare charge are given in figure 7. These times are both close to the time of the initial impact on the roof (700 μsecs). It can be seen that, even close to the time of impact, some of the coolant momentum is directed elsewhere than towards the roof. The directional effect of the confinement is sufficient to increase the duration of the roof loading and produce a final measured impulse greater than in the case of the unconfined charge.

9. UO_2 Vapour Excursion

An earlier paper, (Cowler and Hoskin [13]), has illustrated the differences in damage caused by high explosive charges and UO_2 vapour excursions in simple spherical geometry. It was thought of interest to extend this comparison to a simple 2-D geometry by continuing the present series of calculations, replacing the explosive charge by a UO_2 vapour expansion. The region of lead shot in the model confinement was intended to simulate both the core and breeder sections without explicitly defining the boundary between them. Therefore it is impossible to define the true core volume without making some assumptions about possible modelling of some real reactor system. Such a refinement was not desirable since this could introduce questions of unsatisfactory modelling of other parts of the system. It was therefore decided to allow the region of UO_2 energy release to replace the whole region of lead shot. The initial density of the UO_2 was taken to be uniform at 5 g/cc and the initial energy distribution, similar to those used in the spherical calculations of Cowler and Hoskin [13], was derived from the output of a Bethe-Tait code, PHOENIX (see Hicks and Menzies [14]). The specific profile was chosen so that the energy made available by expanding adiabatically down to a uniform pressure of 1 bar matched the available energy of the explosive charge used in the previous calculations. It again should be emphasized that the calculation was not intended to simulate a true reactor incident but to illustrate the main differences and similarities in loadings arising from the two forms of energy release.

9.1 Results of Calculation

The equation of state used for the expanding UO_2 vapour was one permitting both single phase and two phase behaviour (Morgan [15]). Those for graphite and water were the same as for the explosive charge runs, including the spalling behaviour. Somewhat surprisingly, spalling did occur at the water surface during the incident, although it had not been thought probable for the steadier and slower expansion from the UO_2 vapour. The spalling was not as severe as in the case of the high explosive shot - nevertheless it did occur.

The expansion was much slower than for the explosive charge and a comparison of the impulses at gauge 3 (see figure 10) shows that the loading from explosive was complete before the loading caused by the UO_2 energy release had begun. However the impulse then smoothly increased and when the calculation was stopped at 4 msecs the total impulse at gauge 3 almost exactly equalled that due to the explosive charge.

For the impulse at gauge 11, the centre of the core plug, a similar delay in arrival is apparent. After impact the rate of increase in impulse is very similar to that for the explosive charge showing that the values of the mean fluid velocity towards the roof were similar in both calculations. However the final impulse on the roof is about 25% greater than that arising from the explosive charge.

On close examination of the results it is found that the energy transfer from the UO_2 region to the surrounding regions increases steadily up to about 2½ msecs (i.e. about the time of impact on the roof) but then the rate of energy transfer slows down significantly and when the calculation was stopped at 4 msecs only approximately half of the total available energy had become available. Therefore when comparing the impulses at gauges 3 and 11 we must recognise the differences in energy release from the two types of energy sources. Thus if the impulses are used as a measure of damage potential we can say, in the present geometry (and it would be dangerous to generalise from a single example), that to produce the same damage on the wall with an explosive charge as with UO_2 the energy released

by the explosive needs to be about twice the effective mechanical energy coming from the UO_2 If we are interested in the impulse on the roof then the factor will be somewhat greater than 2. These factors are not significantly different from those determined by Cowler and Hoskin [13] in the simpler 1-D geometry.

10. Conclusions

The results of the calculations, taken together with those of Hoskin et al [5] demonstrate that ASTARTE has the ability to predict with accuracy the loadings and impulses around the walls and roof of a reasonably complicated structure typical of a fast reactor system. However it is obvious that to be able to predict the experimental results with the desired accuracy and confidence it is necessary to model realistically all components and materials within the system. Therefore the development of constitutive relations to describe all the various constituents of a fast reactor system is essential if computer codes are to be used to provide accurate predictions of the dynamic consequences of energy releases, either nuclear or explosive.

The comparison of the impulses arising from the UO_2 and high explosive energy releases indicated that comparative damage potential occurred if the energy releases differed by a factor of about two. This suggests that experiments using explosive with energy releases roughly equal to those of interest for design basis accidents (a factor of two could be included if thought necessary but refinements such as low density explosives should reduce this factor, (Cowler and Hoskin [13])) will give valuable information, either directly to the designers, or as basic data to use in the codes developed or currently under development.

References

[1] FISTEDIS, S.H., "Containment of fast breeder reactors - present status - remaining problems". Proceedings of First International Conference on Structural Mechanics in Reactor Technology Vol. 3 (EUR 4820) 121 (1971).

[2] DOERBECKER, K., Private communication.

[3] ASH, J.E., "The reliability of computer predictions of the hydrodynamics of reactor excursions" Proceedings of First International Conference on Structural Mechanics in Reactor Technology Vol. 3 (EUR 4820) 147 (1971).

[4] HOSKIN, N.E., "The use of computers in investigations on hydrodynamic aspects of reactor safety problems". Proceedings of Conference on Computational Physics (Culham 1969) UKAEA Report CLM-CP part 12.1 (1969).

[5] HOSKIN, N.E., MAWBEY, M.W.S., REES, N.J.M., "Calculation of the dynamic response of reactor containment systems". Proceedings of Conference on Engineering of Fast Reactors for Safe and Reliable Operation (Karlsruhe 1972) Paper 41.

[6] EGLEME, M., NAMIAS, M., HOLTBECKER, H., "Study of Nuclear Accidents by Chemical Simulation Experiments". Ibid. Paper 39.

[7] DENISE, R.P., SPEIS, T.P., FISTEDIS, S.H., CHANG, Y., STEPHENS, D.D., FOX, G.L., FLORENCE, A.L., ABRAHAMSON, G.R., "Containment of fast breeder reactors - recent developments in analytical and experimental methods". Ibid. Paper 45.

[8] REES, N.J.M., "A model investigation of explosion containment in single tank fast reactors" Proceedings of Conference on Safety, Fuels and Core Design in Large Fast Power Reactors (Argonne 1965) USAEC Report ANL-7120 (1965).

[9] WILKINS, M.S., "Calculation of elastic-plastic flow". Chapter 6 Methods in Computational Physics 3 (ALDER, B. et al Eds). Academic Press, New York, USA (1964).

[10] LINDE, R.K., SCHMIDT, D.N., "Shock propagation in non-reactive porous solids", J. App. Phys. 37, 3259 (1966).

[11] HERRMANN, W., "Constitutive equation for the dynamic compaction of ductile porous materials", J. App. Phys. 40, 2490 (1969).

[12] BUTLER, T.D., "LINC method extensions", Proceedings Second Conference on Numerical Methods in Fluid Dynamics (Univ. of Calif., Berkeley 1970), Lecture Notes in Physics, 8, pp 435-440, Springer-Verlag, Berlin (1971).

[13] COWLER, M.S., HOSKIN, N.E., "Comparison of the pressure effects of energy release from nuclear excursions and chemical simulations", Proceeding of Conference on Engineering of Fast Reactors for Safe and Reliable Operation (Karlsruhe 1972) Paper 40.

[14] HICKS, E.P., MENZIES, D.C., "Theoretical studies on the fast reactor maximum accident; Proceeding of Conference on Safety, Fuels and Core Design in Large Fast Power Reactors (Argonne 1965) USAEC Report ANL 7120 (1965).

[15] MORGAN, K., "An expansion equation of state subroutine", Computer Physics Communications 5, 64 (1973).

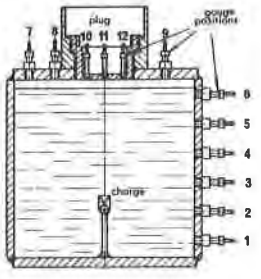

FIGURE 1
CROSS SECTION OF
MODEL REACTOR TANK

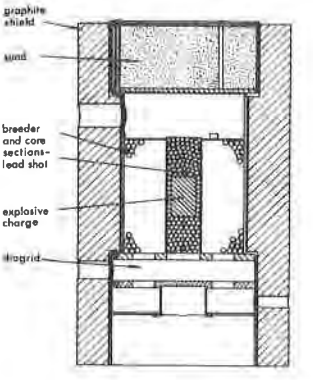

FIGURE 2
CROSS SECTION OF
MODEL CORE AND BREEDER STRUCTURE

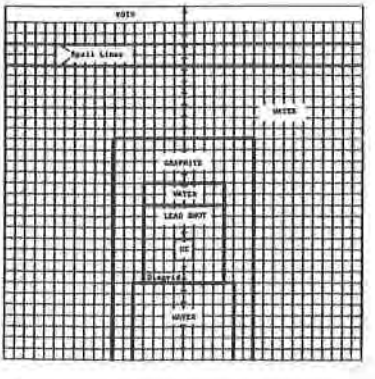

FIGURE 3(a)
INITIAL MESH CONFIGURATION
FOR CALCULATION INVOLVING A CONFINED CHARGE

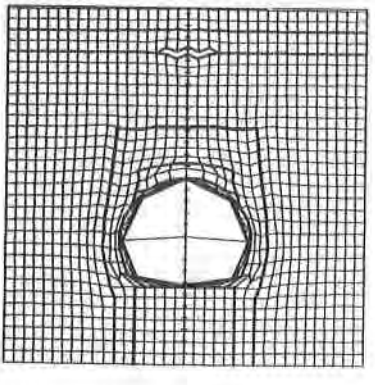

FIGURE 3(b)
DEFORMED MESH SHOWING SPALLING
AT FREE SURFACE OF WATER

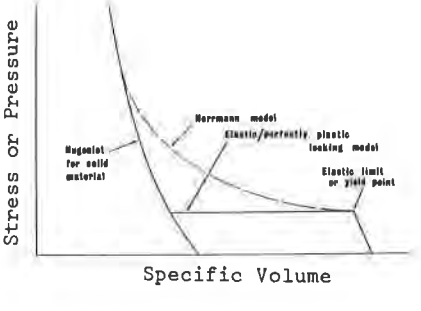

FIGURE 4
HUGONIOT FOR DISTENDED MATERIAL

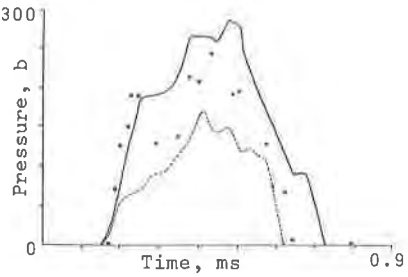

FIGURE 5
EFFECT OF HUGONIOT FOR DISTENDED
MATERIAL ON THE LOADING AT GAUGE 3

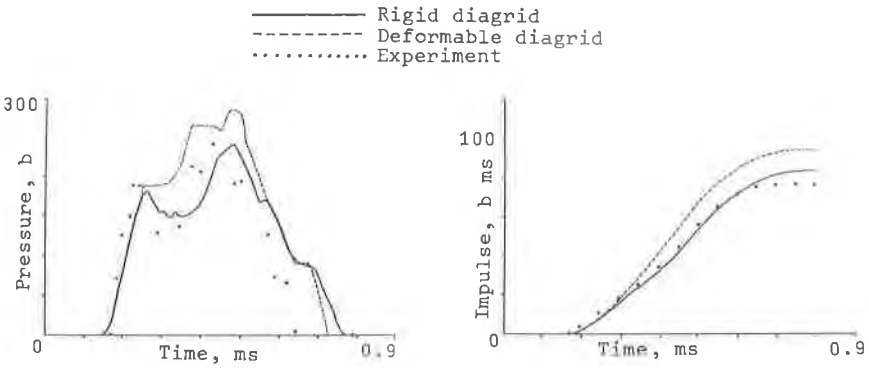

FIGURE 6(a)
EFFECT OF THE DIAGRID ON THE
LOADING AT GAUGE 3

FIGURE 6(b)
EFFECT OF THE DIAGRID ON THE
IMPULSE AT GAUGE 3

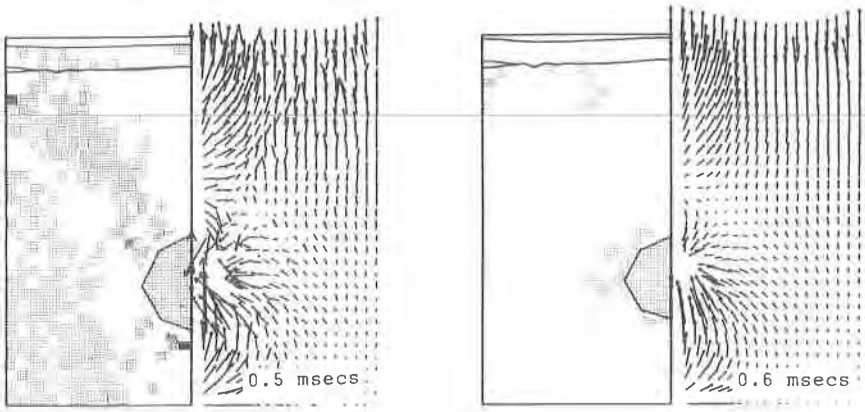

FIGURE 7
PRESSURE AND VELOCITY DISTRIBUTIONS AT TWO EPOCHS
OF THE CALCULATION INVOLVING A BARE CHARGE
(Direction of wave propagation indicated by arrows)

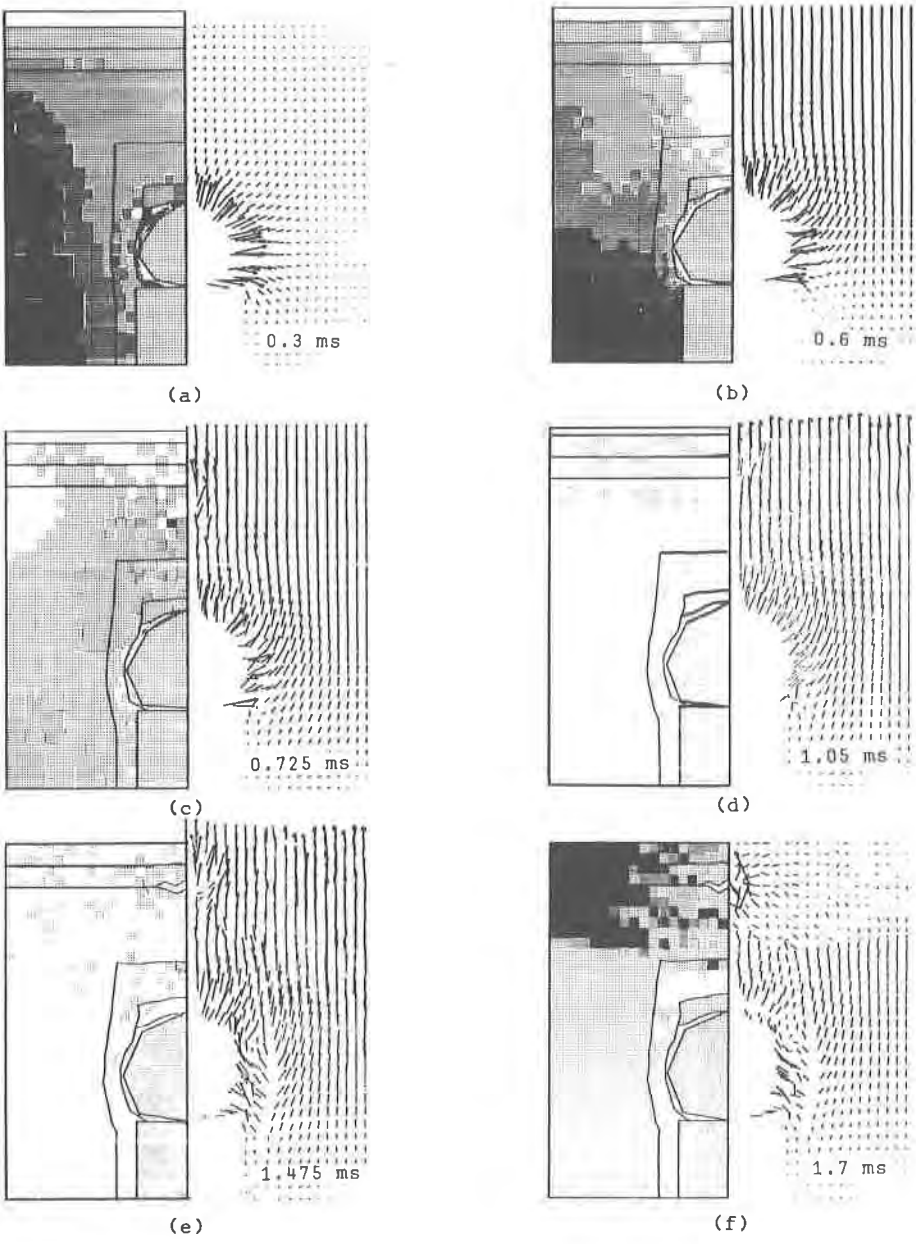

FIGURE 8
PRESSURE AND VELOCITY DISTRIBUTIONS AT SIX EPOCHS
OF THE CALCULATION INVOLVING A CONFINED CHARGE
(Direction of wave propagation indicated by arrows)

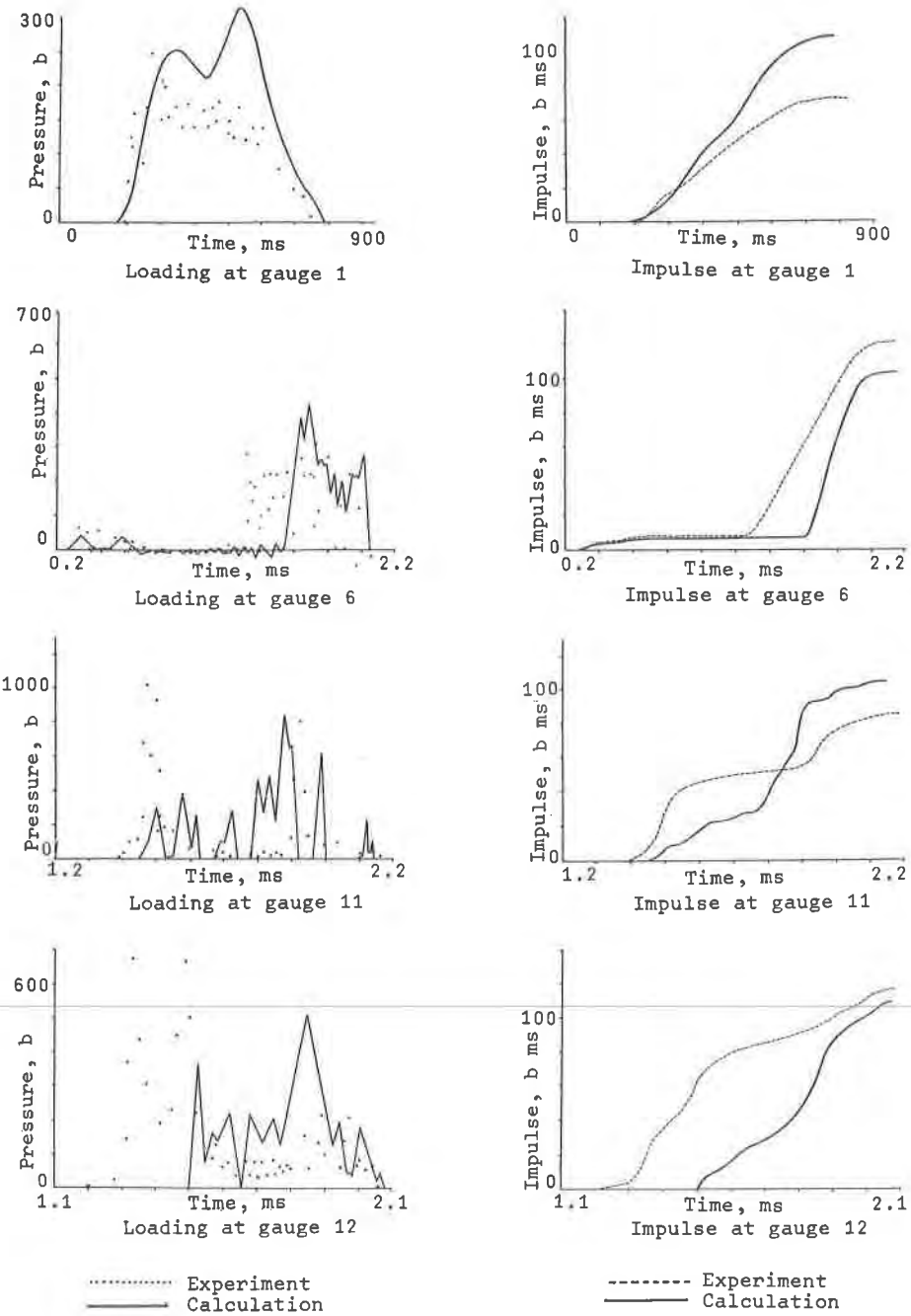

FIGURE 9
COMPARISON OF COMPUTED AND MEASURED LOADING AND IMPULSES FOR THE MODEL TEST INVOLVING A CONFINED CHARGE

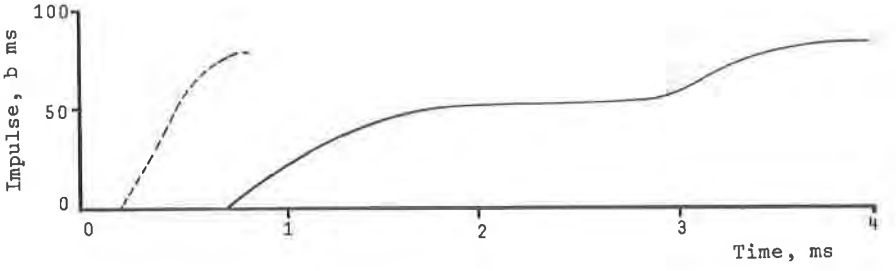

Gauge 3

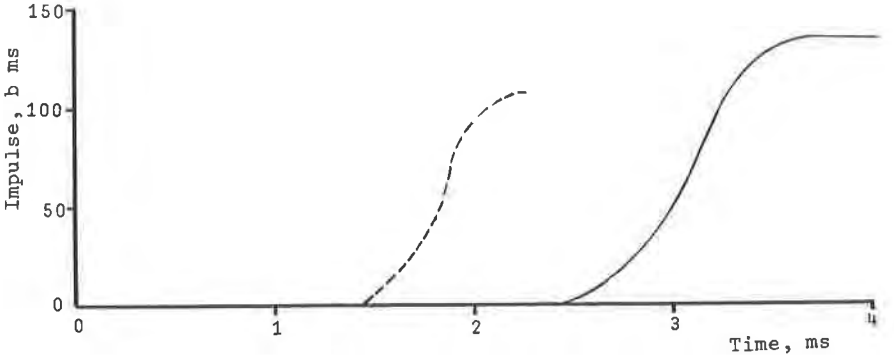

Gauge 11

FIGURE 10
COMPARISON OF COMPUTED IMPULSES AT GAUGE 3 AND GAUGE 11 FOR CALCULATIONS INVOLVING A CONFINED CHARGE AND A UO_2 VAPORISED CORE

------ Confined Charge
—————— Vaporised Core